105 (2026) 106820

Contents lists available at ScienceDirect

Poultry Science

journal homepage: www.elsevier.com/locate/psj

Full-Length Article

Transcriptomic analysis reveals a crucial role of the yolk sac during Avian Pathogenic *Escherichia coli* infection in chicken embryos

Jingyao Wang [a], Yadav Sharma Bajagai [b], Ghulam Asghar Sajid [a], Runsheng Li [a], Surya Paudel [a,c,*]

[a] Department of Infectious Diseases and Public Health, Jockey Club College of Veterinary Medicine and Life Sciences, City University of Hong Kong, Kowloon, Hong Kong SAR, China
[b] School of Health, Medical and Applied Sciences, Institute for Future Farming Systems, Central Queensland University, Rockhampton, Qld 4701, Australia
[c] Jockey Club College of Veterinary Medicine and Life Sciences Research Centre for Applied One Health Research and Policy Advice, City University of Hong Kong, Hong Kong SAR, China

ARTICLE INFO

Keywords:
Escherichia coli
Embryos
Transcriptomic
Yolk sac
Host–pathogen interaction

ABSTRACT

Colibacillosis caused by Avian Pathogenic *Escherichia coli* (APEC) is a major threat to poultry, and yolk sac infection is a leading cause of embryonic mortality. However, the molecular mechanisms and host responses during the infection have not yet been investigated. To address this, we performed RNA-seq to compare the *in vivo* transcriptomic profiles of yolk sac and embryonic liver from APEC-infected embryos in multiple scenarios, including dead, live, and mock-infected controls. In dead embryos, particularly in the yolk sac, marked pro-inflammatory cytokine activity, mitochondrial dysfunction, impaired fatty acid metabolism, and structural disruption were observed. In contrast, surviving embryos exhibited a regulated inflammatory response, enhanced oxidative phosphorylation and fatty acid oxidation, increased expression of antimicrobial peptides, strengthened antioxidant defenses, and tissue repair pathways. While yolk sac and liver responses were positively correlated, the yolk sac displayed greater inflammation and metabolic dysregulation, underscoring its vulnerability. These findings highlight the previously underappreciated role of the yolk sac in APEC pathogenesis and offer avenues to improve host resilience and mitigate losses in poultry production.

Introduction

The global population is projected to reach 9.8 billion by 2050, driving urbanization, and rising affluence that will double the demand for poultry products (Kleyn and Ciacciariello, 2021). However, rapid agricultural intensification presents challenges to healthy, safe, and sustainable poultry production due to higher bird densities, increased stress, greater pathogen transmission rates, and sometimes compromised biosecurity in large-scale operations (Robbins et al., 2016). Embryonic mortality caused by infections with various viruses, bacteria, fungi, and protozoa accounts for over 30 % of all death cases in poultry at an early age. Among these, early embryonic mortality in chickens is primarily linked to APEC infection (Olsen et al., 2012). *E. coli*, a member of the *Enterobacteriaceae* family, is a Gram-negative, rod-shaped, non-acid-fast, and non-spore-forming bacterium. It has a complex reputation regarding its pathogenicity in poultry, and there are limited options for prophylaxis (Palmieri et al., 2023; Paudel et al., 2024). APEC can reside as a normal commensal in birds; however, the infection can also lead to systemic infection, such as airsacculitis, perihepatitis, pericarditis, and peritonitis, collectively known as colibacillosis (Abdelhamid et al., 2023, 2024). In young birds, omphalitis or yolk sac infection is a major contributor to substantial economic losses worldwide due to high mortality and compromised performance during growth.

The development of the chicken embryo during incubation is a highly coordinated and intricate process, involving a series of physiological, biochemical, and morphological cascades (Givisiez et al., 2020). Yolk sac, a pouch-like and well-vascularized membrane structure surrounding yolk, is composed of an endodermal layer that interfaces with the yolk nutrients, a mesodermal layer containing the vascular system, and an outer ectodermal layer (Wong and Uni, 2021). The yolk, rich in proteins and lipids, is a vital nutrient reservoir essential for embryonic growth and development, but also provides an ideal environment for bacterial proliferation (Rezaee et al., 2021). The yolk sac acts as a true

* Corresponding author at: 10-422, 10/F, Jockey Club One Health Tower, City University of Hong Kong, Hong Kong SAR, China.
E-mail address: spaudel@cityu.edu.hk (S. Paudel).

https://doi.org/10.1016/j.psj.2026.106820
Received 24 January 2026; Accepted 17 March 2026
Available online 18 March 2026

biological barrier, protecting the embryo from bacteria in the yolk. Additionally, yolk sac tissue synthesizes antimicrobial peptides, including avian β-defensin 10 (*AvBD10*) during mid embryogenesis, which, together with maternally derived antibodies in the yolk, likely form a multifaceted innate defense that protects against infections until the embryo hatches (Wong and Uni, 2021). A recent histopathological study highlighted the significance of yolk sac composition and integrity for embryo survival, rather than the presence of pathological lesions in internal organs (Rezaee et al., 2021). However, molecular studies on host responses to APEC have primarily focused on adult birds, particularly in the liver, bone marrow, or intestine (Chen et al., 2025; Li et al., 2024). To this end, the molecular role of the embryonic organs during APEC infection remains unexplored. Thus, we profiled the transcriptomes of extraembryonic yolk sac and embryonic liver tissues following APEC infection using RNA sequencing (RNA-seq), which provides highly accurate and sensitive transcriptional profiles at single-nucleotide resolution (Westermann and Vogel, 2021). We characterized gene expression dynamics of both infected-live and infected-dead embryos to link the differential transcriptional changes and unravel the molecular dysregulation associated with embryonic mortality.

Materials and methods

Ethic statement

The study was approved by the Animal Research Ethics Sub-Committee of City University of Hong Kong (AN-STA-00000020) and conducted in accordance with the institutional requirements.

Bacterial strain

The *E. coli* strain EC—O119H4 was isolated from the liver of a diseased chicken (Wang et al., 2025). The affected flock experienced 30 % mortality at 10 days of age. Chicks were presented with clinical signs such as anorexia, dry shanks, pasty vents, and postmortem evidence of hepatitis and omphalitis. For experimental inoculation, the bacterial isolate was cultured in Luria–Bertani (LB) broth at 37 °C with shaking (250 rpm) for 12 h. The overnight culture was subsequently diluted 1:10 in fresh LB medium with the optical density at 600 nm (OD 600) of approximately 0.5. To determine the viable bacterial concentration, the culture was serially 10-fold diluted in sterile phosphate-buffered saline (PBS). Aliquots (100 μL) of each dilution were spread onto MacConkey agar plates and incubated at 37 °C for 24 h. Colonies were enumerated from plates, and the inoculum concentration was calculated as colony-forming units per milliliter (CFU/mL) using the dilution factor and plated volume.

Infection of embryos

Specific pathogen-free (SPF) embryonated chicken eggs were incubated at 37 °C and 65 % relative humidity. On day 12 of incubation, twenty-four eggs in the treatment group were inoculated with 100 μL of *E. coli* suspension containing approximately 5×10^3 CFU/ml via the allantoic sac. Following the same procedure, sixteen eggs in the control group were injected with 100 μL of sterile PBS. All eggs were candled every eight hours to monitor the embryo viability. Nonviable embryos were promptly removed. At 48 h post-infection, all remaining embryos from both groups were dissected, and yolk sac and liver tissues were collected for total RNA extraction. The sampling time point at 48 post-infection was selected based on previous work, which reported peak mortality at 2 days post infection (Rezaee et al., 2021).

Extraction of total RNA

Yolk sac and liver samples from infected-live, infected-dead and negative control embryos were collected in 1 mL of TRIzol reagent (Invitrogen, CA, USA). Tissue homogenization was performed using the Precellys® Evolution Touch homogenizer (Bertin Technologies, France) with ceramic beads at 8000 rpm for two cycles of 30 s each, separated by a 15-second pause. RNA extraction was carried out using the phenol: chloroform:isoamyl alcohol method (25:24:1) (Sigma, USA), followed by isopropanol precipitation (Hammad, 2023). For each group, three biological replicates were used, each derived from a distinct chicken embryo. RNA integrity and quality were assessed using the Agilent TapeStation system (Agilent Technologies, CA, USA). Due to lower RNA integrity number values (RIN = 2.9, 3.3), liver samples from infected-dead embryos were limited to two replicates.

RNA library preparation and sequencing

The mRNA from the collected samples was enriched using poly-T oligo-attached magnetic beads. Non-strand-specific cDNA libraries were constructed using the NEBNext® Ultra II RNA Library Prep Kit for Illumina according to the manufacturer's protocol (New England Biolabs, MA, USA). High-throughput sequencing was conducted on the Illumina NovaSeq platform, generating 150 bp paired-end reads. All RNA samples were processed and sequenced by Novogene Co. Ltd. (Beijing, China).

Differential gene expression analysis

The quality of raw libraries was assessed using FastQC v0.11.8 (Babraham Bioinformatics, UK). Raw data were trimmed with Trimmomatic v0.39 to remove adaptors and low-quality bases (Q-value ≤ 20) (Bolger et al., 2014). The filtered reads were aligned to the reference genome (GenBank assembly accession: GCA_016699485.1) using TopHat2 (version 2.1.1) (Kim et al., 2013). Differential gene expression (DEG) analysis was performed using the edgeR package, with normalization conducted via the trimmed mean of M-values (TMM) method (Robinson et al., 2010). The significant differential expression was defined as FDR ≤ 0.05 and $|\log_2 \text{fold change}| \geq 1$. These criteria were applied to all analyses presented in the manuscript, except for the Ingenuity Pathway Analysis (IPA) cutoff. DEGs correlation-based comparison was performed between the yolk sac and liver to understand the shared and distinct roles of both tissues in infected dead vs. live embryos.

Gene ontology and functional pathway analysis

To investigate the biological significance of DEGs, Gene Ontology (GO) and Kyoto Encyclopedia of Genes and Genomes (KEGG) pathway enrichment analyses were performed using the ClusterProfiler package in R (version 4.5.0) (Yu, 2024). The GO annotations were obtained from the NCBI RefSeq database, and KEGG pathway annotations were retrieved directly from the KEGG database. The bitr function was used to convert gene IDs based on the OrgDb database. The compareCluster function was employed to identify significantly enriched GO terms within the categories of Biological Process (BP), Molecular Function (MF), and Cellular Component (CC). Statistical significance was assessed using a *p*-value threshold 0.05, with multiple testing correction applied via the Benjamini-Hochberg false discovery rate (FDR) method.

Ingenuity pathway analysis (IPA)

To enable pathway analysis in QIAGEN Ingenuity Pathway Analysis (IPA), RNA-seq data were also processed independently using the nf-core/rnaseq pipeline (v3.10.1) with default settings (Ewels et al., 2020). The pipeline was executed with Nextflow (v22.10.6) (Di Tommaso et al., 2017) and included quality control, adapter trimming, alignment to the *Gallus gallus* reference genome (GenBank assembly accession: GCA_016699485.1) using STAR (Dobin et al., 2013), and

gene-level quantification with Salmon (Patro et al., 2017). DEG analysis for IPA input was performed using the DESeq2 (v1.46.0) (Love et al., 2014) in R, applying standard filtering and normalization procedures. A core expression analysis in IPA was performed using the Ingenuity Knowledge Base as the reference set with default parameters. The cutoff value for IPA was an absolute fold change > 4 and an adjusted *p*-value (FDR) < 0.05 for comparisons involving dead embryo, while live and negative control were compared with cutoff value of an absolute fold change >2 and a *p*-value < 0.05. These thresholds were chosen to obtain a sufficient number of genes (not too high or too low) for input into IPA pathway analysis. This adjustment was not used for comparative interpretation of transcriptional response between groups.

Results

Global transcriptional changes in yolk sac and liver

In the yolk sac, across nine biological replicates, about 432 million raw reads were generated, of which about 413 million high-quality reads were retained after filtering. Individual libraries yielded 39.3–61.8 million reads, and mapping rates to the chicken reference genome ranged from 83.2 % to 87.7 % (Supplementary Table S1). Principal component analysis (PCA) revealed a marked transcriptional shift in infected-dead embryos relative to controls, while infected-live clustered more closely with uninfected embryos, suggesting a more regulated response (Fig. 1A). Venn diagram analysis (Fig. 1B) supported this distinction, with the greatest number of DEGs observed between infected-dead and infected-live embryos ($n = 1980$, 1332 upregulated, 648 downregulated, Fig. 1C). A heatmap of the top 1000 most variable genes (Supplementary Fig. 1; Supplementary Table S2) further confirmed distinct clustering of infected-dead embryos, while infected-live and controls remained transcriptionally similar. In infected-live embryos, enrichment analysis identified a significant upregulation of genes involved in fatty acid metabolism, oxidative phosphorylation (OXPHOS), mitochondrial functions (including biogenesis, electron transport, ATP synthesis), glutathione metabolism, and DNA repair, indicating enhanced mitochondrial functions and oxidative stress management (Fig. 1D, E, Supplementary Table S3, S4). These metabolic shifts were accompanied by IPA-predicted activation of anti-inflammatory cytokine signaling, cell viability pathways (e.g., *AKT1, EGF, EIF2*), autophagy, and interferon-mediated immune regulation (Supplementary Fig. 2). Collectively, these results suggest that infected live embryos mounted a controlled immune response characterized by tissue protection and enhanced OXPHOS. In infected-dead embryos, a pronounced cytokine and chemokine storm, along with increased glycolysis, cellular senescence, apoptosis, and excessive extracellular matrix (ECM) deposition were observed. These changes were coupled with significant downregulation of pathways associated with cell cycle regulation (E2F targets, DNA replication, G2/M checkpoints), fatty acid metabolism, and mitochondrial respiration, indicating a collapse of cellular homeostasis and energy metabolism (Fig. 1D, E, Supplementary Table S3, S4). Consistent with a pro-inflammatory M1-like phenotype, IPA analysis (Supplementary Fig. 3) further highlighted the activation of inflammatory cytokine signaling (*IL1A, IL1B, IL6, TNF*), endothelial cell migration, and immune system dysregulation. Notably, the analysis revealed enrichment of signaling networks involved in dysregulated tissue growth, differentiation, and structural remodeling, including pathways commonly implicated in fibrotic and proliferative disorders. These were driven by genes such as *TGFB3, VEGFA, SMAD1*, and *CCL5*. Overall, these results point to a highly inflammatory, metabolically compromised state with features of tissue damage and maladaptive remodeling.

In the liver, a total of 469 million raw reads were generated across the same experimental groups, with 449 million clean reads retained

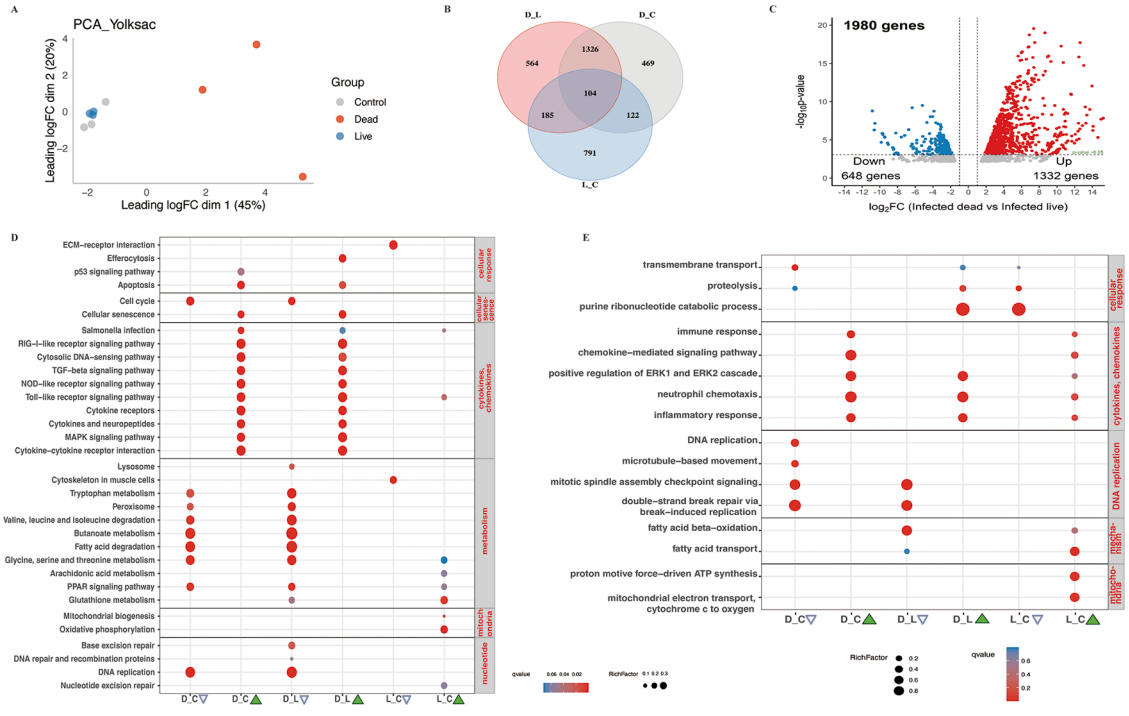

Fig. 1. Transcriptomic analysis of yolk sac tissues during APEC infection in embryonated eggs (A) Principal component analysis plots of the transcriptome profiles of yolk sac in different conditions. (B) Venn diagram showing the overlap of differentially expressed genes (DEGs) among three pairwise comparisons in yolk sac tissue (D_L: infected-dead versus infected-live; D_C: infected-dead versus negative control; L_C: infected-live versus negative control). Transcriptomic reads were mapped to the *Gallus gallus* reference genome using TopHat2, and DEGs were identified using edgeR. Genes with a fold change (FC) ≥ 2 and an adjusted $p \leq 0.05$ were considered significantly differentially expressed. (C) Volcano plot of DEGs between infected dead and live embryos. (D) KEGG pathway enrichment analysis of DEGs, showing condition- and direction-specific enrichment across comparisons. (E) Gene Ontology (GO) enrichment analysis of biological processes for DEGs grouped by comparison and direction.

after quality filtering (49.7–68.7 million per sample). Mapping rates were consistently high, ranging from 88.4 % to 92.0 % (Supplementary Table S5). The PCA revealed strong intra-group consistency and clear separation among infected-dead, infected-live, and control groups, with the infected-dead group showing the most pronounced transcriptional divergence (Fig. 2A, B). A heatmap of the top 1000 most variable genes (Supplementary Fig. 4, Supplementary Table S6) confirmed this pattern, with distinct clustering of dead embryos and tighter grouping of infected-live and control samples, mirroring observations in the yolk sac. DEG analysis revealed extensive transcriptomic reprogramming in infected-dead embryos, with 5659 DEGs (2659 upregulated, 3000 downregulated) relative to infected-live embryos (Fig. 2C).

Infected-live embryos exhibited a controlled transcriptional response in the liver, marked by biosynthetic activation, structural remodeling, and moderate immune engagement. Enrichment analysis revealed upregulation of genes involved in ribosome biogenesis, extracellular matrix, and protein folding, indicating heightened biosynthetic and stress-response activity. In contrast, oxidation-reduction and fatty acid metabolism genes were downregulated, reflecting suppressed oxidative metabolism (Fig. 2D, E). IPA analysis (Supplementary Fig. 5) further supported these findings by highlighting activation of inflammatory and immune-related pathways, including macrophage and myeloid cell activation, leukopoiesis, and lymphopoiesis, driven by genes such as *IFNG, IL1B*, and *TNF*. Additionally, the results suggested increased lipid synthesis (*EGF, IFNG, IL1B, LHCGR*), muscle differentiation and growth (*MYOCD, MRTFB*), and maintenance of blood and immune cell homeostasis (*BCL6, IL1B, TNF*). Compared to the yolk sac, which displayed enhanced mitochondrial function, oxidative phosphorylation, and antioxidant responses, the liver response was more oriented toward protein biosynthesis, tissue development, and hematopoietic activation. This difference suggests a tissue-specific adaptation where the yolk sac supports metabolic resilience, while the liver mobilizes structural and immune capacities to support embryo survival.

In the liver, KEGG analysis revealed that infected-dead embryos showed modest enrichment for cytokine–cytokine receptor interaction, MAPK signaling, and C-type lectin receptor signaling. Downregulated pathways were predominantly metabolic, including oxidative phosphorylation, fatty acid degradation, and peroxisome function (Fig. 2D, Supplementary Table S7). Upregulated genes in both infected-dead vs. control and infected-dead vs. infected-live comparisons were enriched for inflammatory response, intermediate filament, and extracellular matrix organization, indicating tissue remodeling and stress signaling. Conversely, downregulated genes were strongly associated with mitochondrial function, fatty acid β-oxidation, peroxisomal activity, and FAD binding, reflecting a collapse in metabolic and bioenergetic pathways (Fig. 2E, Supplementary Table S8). These findings suggest overactivation and a coordinated shutdown of mitochondrial and metabolic processes in the liver of dead embryos. IPA analysis aligned with these observations, highlighted a dominant immune activation signature driven by key inflammatory mediators such as *IL1B, IL6, TNF, IFNG, and IRF7* (Supplementary Fig. 6). Molecules associated with acute phase response, cytokine signaling, and transcriptional regulation (via *IRF1, IRF3, RELA*) were prominent, along with predicted involvement in autoimmune and inflammatory disease mechanisms. The liver transcriptome of dead embryos also showed activation of pathways related to angiogenesis, tissue remodeling, and cell differentiation, involving genes such as *BMP4, CCN1, PTGS2*, and *FOS*. Additionally, pathways associated with antiviral immunity (*IRF7, MAVS, IFNA2*) and proliferative or malignancy-linked signaling (*IL6, TNF, IL17A*) were activated, reflecting a complex and potentially dysregulated host response. Compared to infected-live embryos, the liver transcriptome in infected-dead embryos showed a shift from balanced immune regulation and biosynthetic activity to widespread inflammation, vascular remodeling, and metabolic collapse, consistent with uncontrolled immune activation and loss of tissue homeostasis.

Hyperinflammation in the yolk sac following APEC infection

The infected-dead embryos exhibited an intense cytokine storm and inflammatory response in the yolk sac. Among the canonical pathways

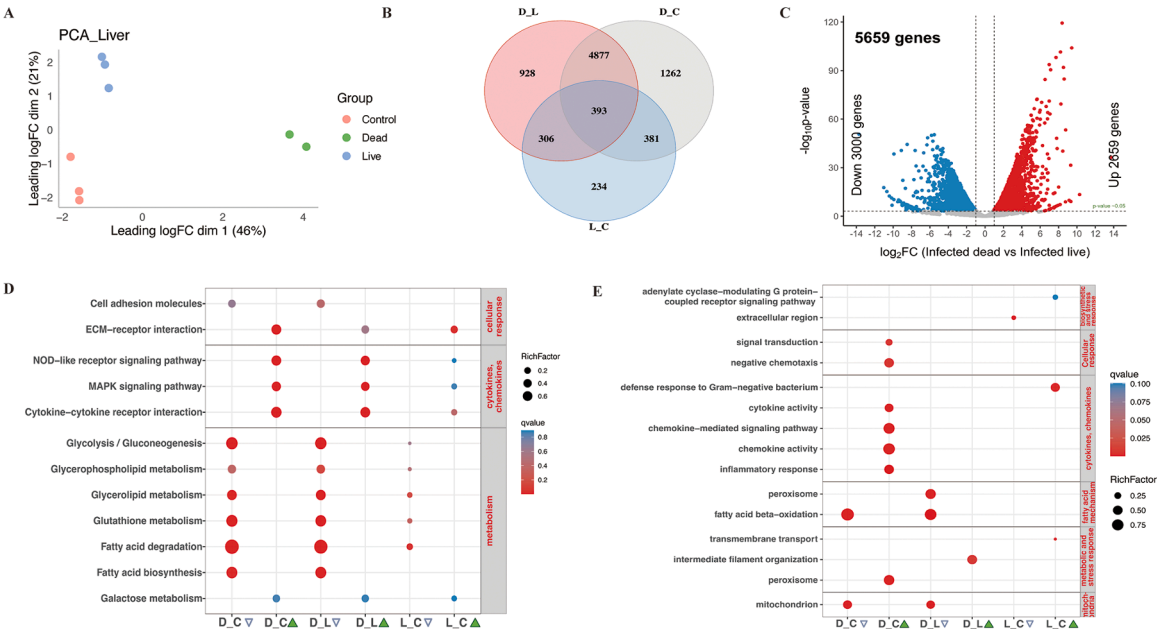

Fig. 2. Transcriptomic analysis of liver during APEC infection in embryonated eggs (A) Principal component analysis plots of the transcriptome profiles of liver in different conditions. (B) Venn diagram showing the overlap of differentially expressed genes (DEGs) among three pairwise comparisons: infected-dead vs. infected-live (D_L), infected-dead vs. uninfected control (D_C), and infected-live vs. uninfected control (L_C). Transcriptomic reads were mapped to the *Gallus gallus* reference genome using TopHat2, and DEGs were identified using edgeR. Genes with a fold change (FC) ≥ 2 and an adjusted $p \leq 0.05$ were considered significantly differentially expressed. (C) Volcano plot of DEGs between infected dead and live embryos. (D) KEGG pathway enrichment analysis of DEGs, showing condition- and direction-specific enrichment across comparisons. (E) Gene Ontology (GO) enrichment analysis of biological processes for DEGs grouped by comparison and direction.

enriched in the yolk sac of infected embryos, the Pathogen-Induced Cytokine Storm Signaling Pathway was the most strongly activated, exhibiting the highest positive activation z-score signaling an intense and dysregulated inflammatory response. The pathway was characterized by broad transcriptional upregulation of several cytokines, chemokines, and inflammation-related mediators (Supplementary Fig. 7). Specifically, genes encoding inflammatory cytokines, including *IL6, IL8L1, IL8L2, IL1B, IL12B, TGFB1*, along with chemokines involved in the chemoattraction of heterophils and monocytes/macrophages, such as *CCL5, CCL19, CCL4, CCLL4, CCL17* and *CX3CL1*, were significantly upregulated in the yolk sac of infected-dead embryos (Fig. 3AI). Furthermore, a significant upregulation of *PTGS2* expression was observed, contributing to a substantial increase in the production of inflammation-associated prostaglandins (Fig. 3AI).

In addition to systemic hyperinflammation, infected-dead embryos displayed elevated expression of genes encoding the coagulation

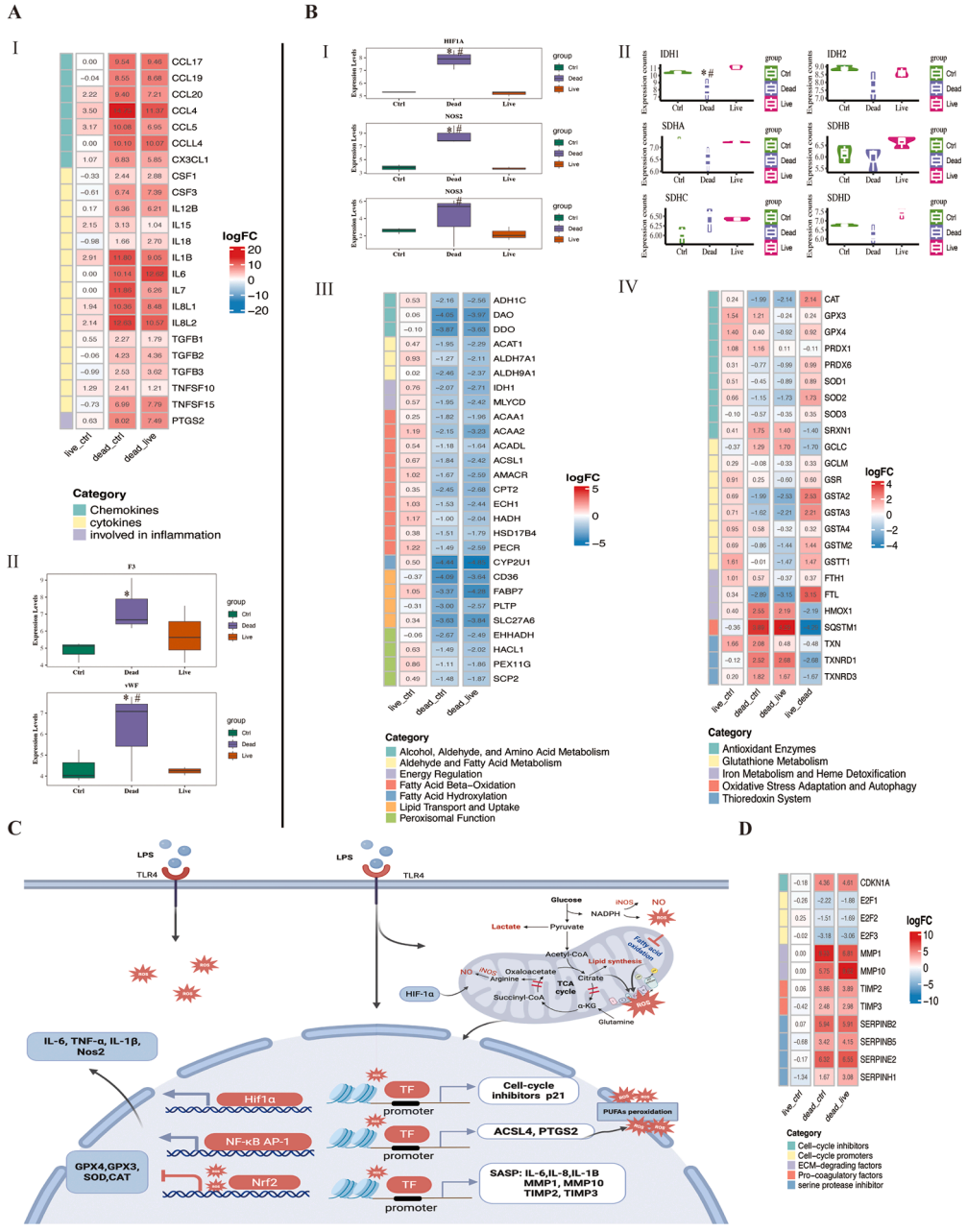

Fig. 3. Transcriptional signatures of the yolk sac in response to APEC infection: inflammation, oxidative stress, and senescence (A) (i) Heatmap displaying $\log_2$ fold changes in the expression of inflammation-associated genes. (ii) Boxplots showing the expression levels (log-normalized counts) of coagulation related genes *F3* and *vWF*. (B) (i) Boxplots showing the expression levels (log-normalized counts) of *HIF1A, NOS2*, and *NOS3*. (ii) Violin plots illustrate the relative expression levels (log-normalized counts) of *IDH* and *SDH* genes involved in the TCA cycle. Gene expression values were normalized using the trimmed mean of M-values (TMM) method in edgeR. Ctrl: negative control; Dead: infected-dead; Live: infected-live. (iii) Heatmap of genes involved in fatty acid metabolism. All heatmap values represent $\log_2$ fold changes between the indicated conditions. (iv) Heatmap showing transcripts associated with the antioxidative stress response. (C) Summary of host transcriptional responses in the dead yolk sac, highlighting hyperinflammation, oxidative stress and cellular senescence following APEC infection. (D) Heatmap showing $\log_2$ fold changes in genes associated with cellular senescence. Asterisks (∗) indicated statistically significant differences between APEC-infected (Dead or Live) and mock-infected groups, whereas hash symbols (#) indicate statistically significant differences between infected-dead and infected-live groups (absolute fold change ≥ 2 and FDR-adjusted $p \leq 0.05$). Pairwise comparisons were performed using edgeR's negative binomial exact test, and p values were adjusted for multiple testing using the Benjamini–Hochberg procedure to control the false discovery rate (FDR).

activator tissue factor (*F3*), indicating a procoagulant phenotype. Similarly, Willebrand Factor (*vWF*), a marker associated with sepsis severity, was also dysregulated (Fig. 3AII). Importantly, this pronounced inflammatory and procoagulant response were uniquely observed in infected-dead embryos, suggesting a strong association with sepsis-like pathology. In contrast, infected-live embryos displayed a resolved immune transcriptomic profile, characterized by the normalization of immune-related gene expression.

Mitochondrial dysfunction and metabolic reprogramming in the yolk sac

APEC infection significantly activated glycolysis-related pathways while concurrently suppressing mitochondrial OXPHOS and fatty acid oxidation in the yolk sac of infected-dead embryos (Fig. 1C, D). This metabolic reprogramming appeared to be driven by hypoxia-inducible factor 1-alpha (*HIF1A)*, a transcription factor typically activated under hypoxic conditions. Notably, *HIF1A* expression was upregulated sixfold in deceased embryos relative to negative controls (Fig. 3BI). In addition, genes encoding key tricarboxylic acid (TCA) cycle enzymes, isocitrate dehydrogenase *(IDH)* and succinate dehydrogenase *(SDH),* were downregulated in infected-dead embryos (Fig. 3BII). The nitric oxide synthase gene *NOS2* was overexpressed by 35-fold (Fig. 3BI), leading to excessive nitric oxide (NO) generation and a concomitant increase in *IL6* expression, further amplifying oxidative stress and inflammation (Sweet et al., 2025). LPS notably impacted lipid metabolism, as the PPAR signalling pathway (Supplementary Fig. 8) and arachidonic acid metabolism were significantly suppressed in infected-dead embryos (Fig. 1C, D). Fatty acid oxidation, including both mitochondrial and peroxisomal β-oxidation was markedly reduced (Fig. 1C, D), which are reported to be essential for degrading very long-chain fatty acids. Specifically, genes associated with fatty acid uptake (*FABP7*), transport (*CPT2, CD36, SLC27A6*), and oxidation (*ACAT1, ACAA2, ACADL, ECH1*) were significantly downregulated (Fig. 3BIII), resulting in lipid accumulation and impaired mitochondrial function. The downregulation of mitochondria-associated genes (Supplementary Fig. 9), coupled with impaired ATP production, indicated mitochondrial dysfunction and elevated reactive oxygen species (ROS) accumulation (Fig. 3C).

In infected-live embryos, fatty acid metabolism and OXPHOS were enhanced, and glutathione-dependent ROS detoxification pathway was activated, as demonstrated by the significant upregulation of glutathione peroxidases (GPX4, GPX3) and glutathione S-transferases (GSTT1). Furthermore, the expression of key antioxidant enzymes, including superoxide dismutase (SOD) and catalase (CAT), was markedly increased (Fig. 3BIV), facilitating efficient ROS neutralization and protection against oxidative stress. Conversely, infected-dead embryos exhibited increased expression of thioredoxin reductase 1 (TXNRD1) (Fig. 3BIV), with both antioxidant function and known association with age-related inflammation (Yang et al., 2024).

DNA damage and cell senescence during yolk sac infection

Cellular senescence and cell cycle arrest were the key transcriptomic features in the yolk sac of infected-dead embryos (Fig. 1C, D), driven by the DNA damage and activation of the p53–p21 axis, which repressed cell cycle genes (Rossiello et al., 2014). In contrast, the infected-live embryos upregulated DNA repair pathways, indicating a self-protective response. Among the most prominently upregulated host transcripts in the yolk sac, ECM-degrading enzymes *MMP1* and *MMP10* exhibited more than a 100-fold increase in expression (Fig. 3D), while *PTGS2* demonstrated a striking 180-fold upregulation (Fig. 3AI), contributing to elevated prostaglandin E2 (*PGE2*) production. Additionally, a profound overexpression of pro-inflammatory cytokines was observed, with *IL1, IL6*, and *IL8* each showing over 1000-fold increase (Fig. 3AI). Concurrently, serine/cysteine protease inhibitors (SERPINs) were upregulated by 60-fold, accompanied by the induction of tissue inhibitors of metalloproteinases (TIMPs) (Fig. 3D). Collectively, these factors constitute the senescence-associated secretory phenotype (SASP), a pro-inflammatory transcriptional program that may contribute to the development of both cytokine storm and tissue fibrosis (Gorgoulis et al., 2019). Moreover, upregulated p21 inhibited CDK–cyclin activity, while downregulated E2F factors reinforced cell cycle arrest, and possibly prevented DNA replication initiation (Fig. 3D).

Metabolic and detoxification responses of embryonic liver during APEC infection

APEC infection led to significant metabolic dysregulation in the embryonic liver, with distinct patterns between infected-live and infected-dead embryos. Infected-dead embryos showed marked downregulation of fatty acid β-oxidation genes, including *ACSL1, ACADL*, and *CPT1A* (Fig. 4A; Supplementary Table S6), indicating impaired fatty acid uptake and mitochondrial oxidation. Similarly, key components of mitochondrial oxidative phosphorylation (*SDHB, NDUFA9, COX5A*) were downregulated in both infected groups, suggesting reduced ATP production and compromised mitochondrial function (Fig. 4A). Peroxisomal genes showed mixed regulation, while *PEX11A* was upregulated, *ABCD3* and *ACOX1* were suppressed, indicating disrupted peroxisomal metabolism and fatty acid processing. Antioxidant genes, such as *CAT,* were significantly downregulated. Interestingly, *GPX1* was modestly upregulated, possibly reflecting a compensatory antioxidant response (Fig. 4A). These findings highlight a failure of metabolic and oxidative homeostasis in the embryonic liver of infected-dead embryos.

The role of antimicrobial peptides (AMPs) in embryonic survival

The expression of avian β-defensins, particularly *AvBD9* and cathelicidins such as *CATH2*, was found to be upregulated in yolk sacs of infected-live embryos, whereas such induction was absent in infected-dead (Fig. 4B). It highlighted the potential impact of host metabolic status on AMP regulation within yolk sac. Interestingly, liver tissues of both infected-live and infected-dead embryos exhibited upregulation of defensins such as *AvBD6* and *AvBD7*, and cathelicidins including *CATH1* and *CATH2*, compared to control groups (Fig. 4B) suggesting that liver may retain structural and functional integrity sufficient for antimicrobial peptide expression even after embryos were dead.

Roles of the yolk sac and liver in structural integrity and metabolic activity

We compared the transcriptional profiles of the yolk sac in relation to the liver from infected-live and infected-dead embryos. A total of 12466 genes were assessed for expression changes. Among these, 1207 genes were considered significant DEGs based on earlier criteria (FDR ≤ 0.05 and $\log_2$FC ≥ 1) in both tissues, while 564 and 3694 genes were significant only in the yolk sac or the liver, respectively. Most of the genes ($n = 7002$) were not differentially expressed in either tissue. Among the 1207 significant DEGs shared between both tissues, 732 were upregulated, 404 were downregulated, 52 were upregulated in the yolk sac but downregulated in the liver, while only 19 DEGs were upregulated in the liver but downregulated in the yolk sac (Fig. 5A, Supplementary Table S9).

To evaluate the similarity in transcriptional responses between the yolk sac and liver, Pearson correlation analysis was performed on the $\log_2$ fold changes ($\log_2$FC) of genes in the infected-dead vs infected-live embryos (Fig. 5B). Pearson correlation analysis revealed a significant positive correlation between log fold changes in yolk sac and liver ($r = 0.531$, $p < 2.2 \times 10^{-16}$). The 95 % confidence interval for the correlation coefficient ranged from 0.518 to 0.543, indicating a moderate and statistically robust association in gene expression changes between these two tissues.

About 60 % of DEGs in the yolk sac overlapped with those in the liver when comparing infected-dead vs. infected-live embryos, but the fold change was largely greater in the yolk sac (Fig. 5C, D, Supplementary

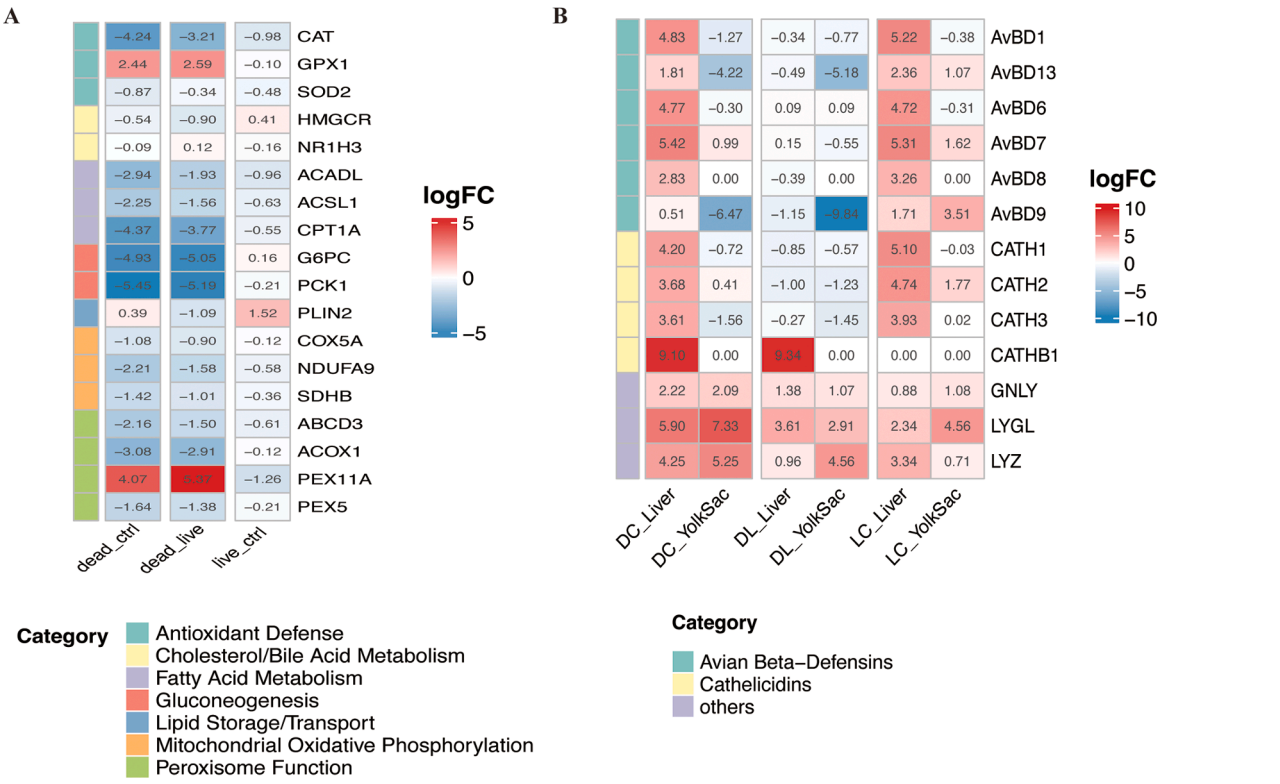

Fig. 4. Heatmap compassion of antimicrobial peptides, metabolism and oxidative stress in the yolk sac and the liver in response to APEC infection (A) Dysregulation of genes involved in metabolic and stress response pathways. (B) Differential expression of genes associated with antimicrobial peptides (AMPs). Comparisons include D_C (infected-dead vs. uninfected control), L_C (infected-live vs. uninfected control), and D_L (infected-dead vs. infected-live). All heatmap values represent $\log_2$ fold changes in gene expression between the indicated conditions.

Table S9). This indicates a stronger inflammatory response in the yolk sac despite its lower number of DEGs. Both tissues showed suppression of fatty acid degradation, glutathione metabolism, and mitochondrial biogenesis, but these effects were less pronounced in the liver. Liver-specific upregulated genes revealed increased expression of arginase-2 (*ARG2*), interleukin-10 (*IL10*), interleukin 1 receptor type 2 (*IL1R2*), transcription factors *IRF4,* which are known to facilitate tissue repair and anti-inflammatory signalling (Supplementary Table S9).

The functional analysis of (i) upregulated in yolk sac but downregulated in liver (significant in both tissue and/or at least yolk sac) and ii) upregulated in embryonic liver but downregulated in yolk sac (significant in both tissue and/or at least embryonic liver), revealed distinct biological roles of each tissue in the embryonic death. Key pathways among top enriched KEGG pathways (Supplementary Table S10), glycosaminoglycan binding proteins, proteoglycans, focal adhesion, and ECM-receptor interaction pathways are directly related to ECM structure and cell adhesion during both dead or live conditions in first group of DEGs such as *COL18A1, COL4A5, CD82, VEGFRKDRL, AGRN, ESM1*, and *GPC2* (Fig. 5E). While in the second group key functional pathways were ribosomes, mitochondrial biogenesis, Wnt signaling pathways, cytokine-cytokine receptor interaction and lysosome with the upregulation of the DEGs of RPL family genes with others like *MRPL49, CTSE* and *CTSH* (Fig. 5F, Supplementary Table S9, S10), indicating that the tissue integrity mechanisms were more active in the yolk sac and anti-inflammatory and metabolic activity were enhanced in the liver.

Discussion

APEC infection in hatching eggs can lead to acute septicemia, with the yolk sac identified as a primary site of bacterial colonization and multiplication, often resulting in embryonic mortality. APEC infection in embryos represents a systemic process; however, this study focused on the yolk sac and liver, as representatives of embryonic and extra-embryonic tissues. The yolk sac, as the primary site of nutrient exchange and early pathogen exposure, and the liver, as a key metabolic and innate immune organ, were selected. So far, the molecular mechanisms and tissue-specific host responses underlying embryonic death are poorly understood. This study presents a comprehensive transcriptomic analysis of chicken embryonic responses to APEC infection, revealing differences between embryos that survived and those that succumbed to it. By profiling transcriptomes in both the yolk sac and embryonic liver, we identified distinct yet interconnected immune and metabolic pathways that underpin resistance or susceptibility to APEC-induced mortality. Although a significant positive correlation was observed in gene expression changes between the yolk sac and liver, the yolk sac exhibited a more intense inflammatory and degenerative profile, whereas the liver demonstrated a relatively balanced response involving immune regulation and structural remodeling. This study highlights the pivotal roles of mitochondrial dysfunction, hyperinflammation, immune dysregulation, oxidative stress, and impaired AMP signaling in determining embryonic survival. Furthermore, our findings demonstrate that the outcome of APEC infection depends not only on the presence of inflammation, but also on the tissue's capacity to sustain metabolic resilience, maintain inflammatory homeostasis, and preserve structural integrity.

In our study, dysregulated expression of genes involved in the suppressed TCA cycle, enhanced glycolysis, and upregulated *HIF1A* suggests a hypoxic microenvironment in the yolk sac of infected-dead embryos. *HIF1A*, a central transcriptional regulator under hypoxia, is known to promote pro-inflammatory cytokine expression, repress fatty acid oxidation, and inhibit electron transport chain (ETC) activity (Taylor and Scholz, 2022). Notably, in infected-dead embryos, we observed downregulation of mitochondria-associated genes and reduced ATP production, indicative of mitochondrial dysfunction and oxidative

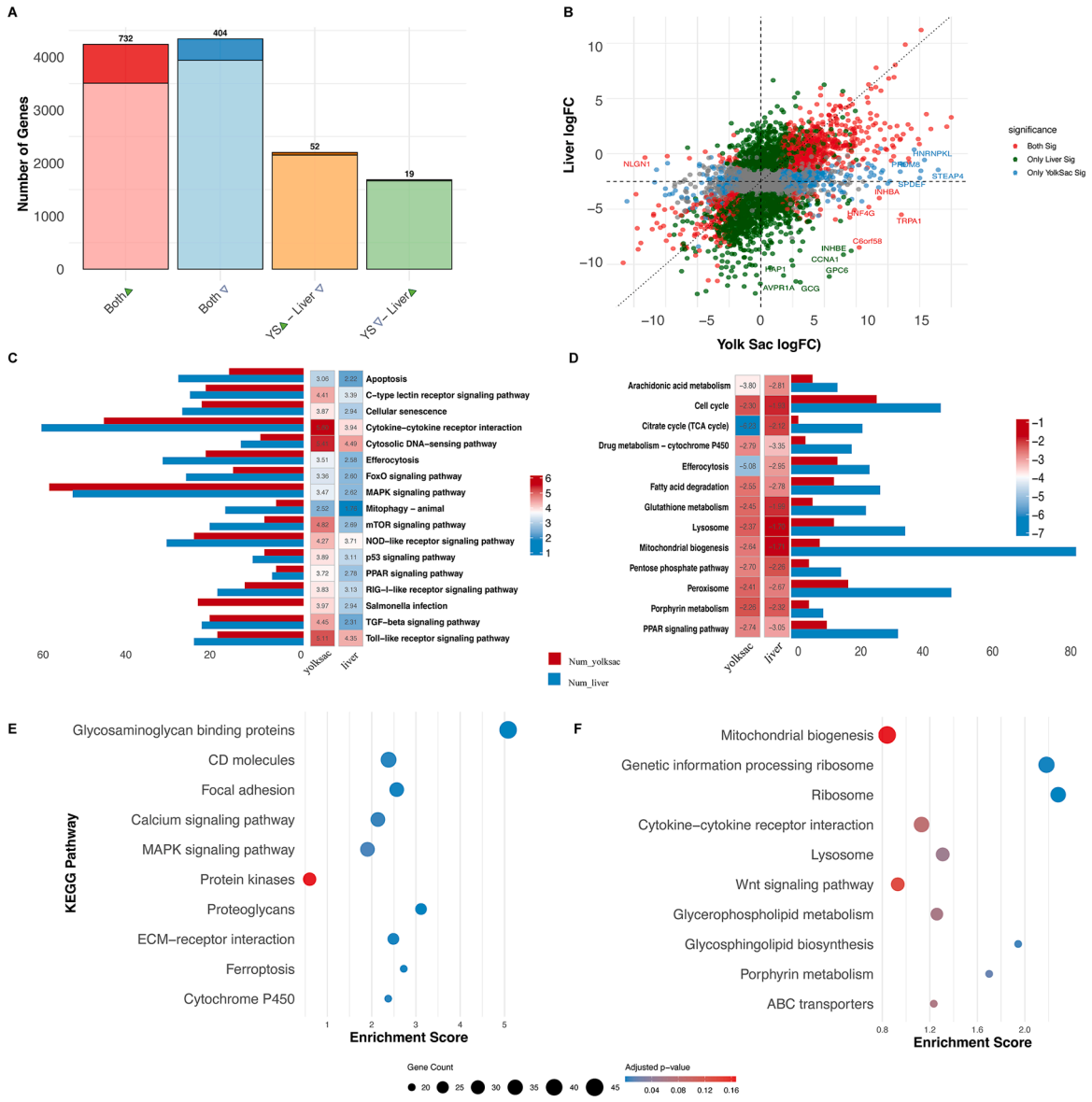

Fig. 5. Tissue-specific transcriptional divergence between the yolk sac and the liver during APEC infection (Infected dead vs infected live embryo) (A) Bar plot of all expressed genes is colored based on their regulation of expression pattern: upregulated in both tissues (red), downregulated in both (blue), up in yolk sac and down in liver (orange), and down in yolk sac and up in liver (green), while the significant DEGs present in each group stacked on each bar with relative numbers. (B) Scatter plot of gene expression log2 fold changes in yolk sac (x-axis) and liver (y-axis) for each gene (n = 12,467), illustrated significant genes in each group. (C) Heatmap illustrating the mean log_2-fold change of upregulated genes in the key KEGG pathways, in dead versus live condition. Bar plots display DEG counts, with liver in blue and yolk sac in red. (D) Heatmap illustrating the mean log_2-fold change of downregulated genes in the key KEGG pathways, in dead versus live condition. Bar plots display DEG counts, with liver in blue and yolk sac in red. (E) Functional pathway enrichment analysis of DEGs upregulated in yolk sac but downregulated in embryonic liver (significant in both tissue and/or at least yolk sac). (F) Functional pathway enrichment analysis of DEGs upregulated in embryonic liver but downregulated in yolk sac (significant in both tissue and/or at least embryonic liver).

stress. Severely damaged mitochondria may further contribute to pathology by releasing excess ROS and mitochondrial DNA (mtDNA), thereby promoting inflammatory necrosis and cell death (Iba et al., 2025). Suppressed OXPHOS, along with elevated levels of NO and pro-inflammatory cytokines, as well as impaired fatty acid oxidation, likely contribute to ETC dysfunction and further ROS accumulation. However, direct functional assays will be required to confirm whether these transcriptional changes translate into measurable mitochondrial impairment. In addition, the downregulation of *FABP7*, a key mediator of polyunsaturated fatty acid (PUFA) uptake and lipid droplet formation, may exacerbate lipid peroxidation and membrane instability (Islam et al., 2019). Excessive ROS, in turn, damages mitochondrial components, degrades ETC complexes, and amplifies inflammatory signalling, establishing a self-perpetuating cycle of mitochondrial injury and inflammation (Morris et al., 2022). This is further supported by increased oxidative stress markers, including TBARS and ROS, observed in breeder chicks after APEC infection (da Rosa et al., 2020). Sustained oxidative stress also promotes cellular senescence and DNA, telomere damage, impairing mitochondrial function, and activating cell cycle arrest pathways (Wiley et al., 2016). Previous studies showed that APEC infection resulted in observable DNA damage (as assessed by comet assay), elevated levels of oxidative stress marker malondialdehyde (Hashem et al., 2022; Hu et al., 2023) and senescence-associated biomarker SA-β-galactosidase induced by LPS in real-world settings (Chen et al., 2023). Collectively, these findings suggest that in dead embryos, mitochondrial dysfunction and cytokine signalling initiate a

self-amplifying cycle of oxidative stress and hyperinflammation in the yolk sac, ultimately contributing to the inflammatory cell death and embryo mortality.

It is well established that lipids, which constitute approximately 60 % of the yolk's dry weight (Speake et al., 1998), are essential for embryonic development, with the yolk sac serving as a central site for their uptake and utilization (Shibata et al., 2023). During infection, the elevated ROS levels during infection can oxidize PUFAs into lipid peroxides (LPO), thereby amplifying oxidative damage (Yang and Stockwell, 2016). The concurrent upregulation of *ACSL4* and *PTGS2* together with the dysregulation of detoxification pathways, highlights the probability of activation of PUFA peroxidation in response to oxidative stress. This is further supported by the observation of yolk sac atrophy during late embryogenesis, likely driven by oxidative stress and ferroptosis, potentially mediated by dysregulation of *ACSL4* and *GPX4* (Liu et al., 2024). Moreover, *PTGS2*, a well-established marker of lipid peroxidation, was markedly upregulated in the yolk sac from the dead embryos (Tang et al., 2021).

Our findings present a compelling model in which the yolk sac acts as an immunological first responder, absorbing the brunt of the inflammatory response that is essential for early host defense during APEC infection while regulating its cellular integrity. This is consistent with previous studies showing that APEC infection triggers rapid recruitment and activation of heterophils and macrophages at the infection site (Abdelhamid et al., 2024; Garcia et al., 2021). However, this protective role comes at a physiological cost: lipid-rich membranes become targets of ROS-induced peroxidation, hyperinflammation, cell death, and ultimately structural collapse. Furthermore, in dead embryos, even though the cytokine activity and AMP production were upregulated in the liver, it failed to compensate for compromised yolk sac functions, highlighting the yolk sac's primacy in survival.

In our previous study, histopathological examination revealed that yolk sacs from dead embryos exhibited marked congestion and inflammation, vascular injury, and abnormal endodermal epithelial cell morphology, compared to surviving embryos (Rezaee et al., 2021). Our results aligned with a previously established hypothesis that the structural and functional integrity of the yolk sac is crucial for embryo survival. This is supported by comparative (cumulative and district) analysis of transcriptomic profiles between the yolk sac and embryonic liver. Collagen-related proteins such as COL18A1 & COL4A5 and FN1 are part of ECM across various tissues. COL18A1 is also essential for vascular integrity (Byron et al., 2013; Khoshneviszadeh et al., 2024). Pathways such as focal adhesion and calcium signaling, including genes like *PDGFA* and *CD82* and *VEGFRKDRL*, suggest roles in vascular development and angiogenesis. Given that the yolk sac vascular network is essential for nutrient absorption (Starck, 2021), its degradation likely compromises embryonic survival. Furthermore, ECM components like proteoglycans and glycoproteins control immune regulation by sequestering cytokines and growth factors (Karamanos et al., 2021). The vulnerability of the yolk sac likely stems from intense inflammatory signaling, mitochondrial dysfunction, oxidative stress, inflammatory cell death, excessive lipid peroxide formation, and disruption of cytoskeletal and structural integrity (Morris et al., 2022; Speake et al., 1998). These findings showed that the biochemical and structural integrity of the yolk sac plays a critical role in the survival of the chicken embryo.

AMPs are critical components of the host's innate immune defense against *E. coli*, primarily by disrupting the integrity of bacterial cell walls (Cuperus et al., 2013). The defensin expression was negatively influenced by increasing aliphatic hydrocarbon chain length of free fatty acids, likely through multiple signaling pathways (Fu et al., 2023). Previous studies have demonstrated that CATH2 (Hao et al., 2024) and CATH-1(6–26) inhibited infection, while ABD1 conferred significant protection against early chick mortality caused by APEC-induced yolk sac infection (Nguyen et al., 2021). These findings underscore the vital role of AMPs in controlling infectious diseases in poultry, and their promising potential as alternatives to antibiotics. In addition, balancing immune response, including pro- and anti-inflammatory cytokines, is crucial for mitigating immunopathology and promoting tissue repair (Ye et al., 2025). The identification of protective mechanisms, such as AMP expression and antioxidant response provides a roadmap for future interventions. Nutritional or pharmacological strategies aimed at boosting mitochondrial function, or enhancing AMP production may improve survival outcomes in poultry.

While the study offers valuable insights, it is not without limitations. RNA from embryonic liver samples showed partial degradation (reduced RIN), which may increase technical variability, introduce 3′-end coverage bias, and reduce sensitivity for detecting differential expression, especially for long transcripts and isoform-level analyses. In addition, the relatively small sample size may limit statistical power and generalizability. Nevertheless, overall sequencing quality was high: more than 90 % of bases achieved Q30, over 88 % of reads mapped to the reference genome, PCA revealed clear clustering by experimental group, and normalized gene-expression profiles showed strong concordance among biological replicates within the dead-liver group (Pearson's $r \geq 0.9$). Although stringent statistical thresholds were applied, validation through larger studies and protein-level assays (e.g., by Western blotting, proteomics) is necessary. Moreover, functional validation of candidate pathways was beyond the scope of this study. Also, higher cut-off values were used for the comparisons involving dead embryos, compared to live and negative control, to keep a reasonable number of genes for the analysis. Because distinct fold-change thresholds were applied during IPA gene list selection, pathway results are interpreted as enrichment within each biological comparison rather than as direct quantitative comparisons of pathway activation magnitude across groups. A further limitation is the use of a single APEC strain for infection. Although this strain is well-characterized and exhibits established virulence traits associated with avian colibacillosis, APEC represents a genetically diverse pathotype. Host transcriptional responses may vary depending on strain-specific virulence factors and genetic background. Therefore, further comparative studies involving multiple pathogenic and commensal *E. coli* strains would be necessary to determine whether conserved or strain-specific host response patterns exist.

Conclusions

This study provides critical insights into host responses in the yolk sac and liver from embryos infected with APEC. Through comparative transcriptomic analysis, we revealed that embryonic mortality is linked to exacerbated inflammation, mitochondrial dysfunction, lipid acid metabolic and cell cytoskeleton disruption, particularly in the yolk sac. In contrast, surviving embryos mounted a coordinated immune and metabolic response, characterized by enhanced mitochondrial function, fatty acid oxidation, and antimicrobial and tissue repair pathways. Mitochondrial oxidative phosphorylation, balanced inflammatory responses, lipid metabolic activity, and yolk sac integrity are crucial for embryo survival. The yolk sac displayed greater inflammation and metabolic dysregulation than the liver. The pronounced vulnerability of the yolk sac underscores its central role in disease progression. These findings not only advance our understanding of APEC pathogenesis at the embryonic stage but also suggest potential targets for improving resistance and reducing economic losses in poultry production.

Data availability

The datasets supporting the conclusions of this article are provided in the manuscript and as supplementary material. The RNAseq data in our paper are available in the GEO repository, accession number: GSE300118.

Funding information

Surya Paudel received the Early Career Scheme grant from the Research Grant Council, Hong Kong (Grant # 21102424, CityU reference # 9048292) and the Startup grant from City University of Hong Kong (Grant # 9610582) to conduct this study.

CRediT authorship contribution statement

Jingyao Wang: Writing – review & editing, Writing – original draft, Visualization, Validation, Software, Methodology, Investigation, Formal analysis, Data curation. **Yadav Sharma Bajagai:** Writing – review & editing, Validation, Formal analysis. **Ghulam Asghar Sajid:** Writing – review & editing, Methodology, Formal analysis. **Runsheng Li:** Writing – review & editing, Validation, Supervision, Software, Project administration. **Surya Paudel:** Writing – review & editing, Supervision, Resources, Project administration, Methodology, Funding acquisition, Conceptualization.

Disclosures

The authors declare that this research was carried out without any commercial or financial affiliations that could be interpreted as a possible conflict of interest.

Supplementary materials

Supplementary material associated with this article can be found, in the online version, at doi:10.1016/j.psj.2026.106820.

References

Abdelhamid, M.K., Hess, C.., Bilic, I., Glösmann, M., Rehman, H.U., Liebhart, D., Hess, M., Paudel, S., 2024. A comprehensive study of colisepticaemia progression in layer chickens applying novel tools elucidates pathogenesis and transmission of Escherichia coli into eggs. Sci. Rep. 14, 8111. https://doi.org/10.1038/s41598-024-58706-3.

Abdelhamid, M.K., Nekouei, O.., Hess, M., Paudel, S., 2023. Association between load in the gut and body weight gain in broiler chickens: a systematic review and meta-analysis. Avian Dis. 67, 298–304.

Bolger, A.M., Lohse, M.., Usadel, B., 2014. Trimmomatic: a flexible trimmer for Illumina sequence data. Bioinformatics 30, 2114–2120. https://doi.org/10.1093/bioinformatics/btu170.

Byron, A., Humphries, J.D., Humphries, M.J., 2013. Defining the extracellular matrix using proteomics. Int. J. Exp. Pathol. 94, 75–92. https://doi.org/10.1111/iep.12011.

Chen, J., Chen, X.Y., Cong, X.X., Wang, S., Xu, S.B., Sun, Y.T., Zhou, Y.T., Zheng, L.L., Huang, M., 2023. Cellular senescence implicated in sepsis-induced muscle weakness and ameliorated with metformin. Shock 59 (4), 646–656. https://doi.org/10.1097/SHK.0000000000002086.

Chen, M., He, Y., Jia, Y., Wu, L., Zhao, R., 2025. Liver transcriptome response to avian pathogenic Escherichia coli infection in broilers with corticosterone treatment. Poult. Sci. 104, 105020. https://doi.org/10.1016/j.psj.2025.105020.

Cuperus, T., Coorens, M., van Dijk, A., Haagsman, H.P., 2013. Avian host defense peptides. Dev. Comp. Immunol. 41, 352–369. https://doi.org/10.1016/j.dci.2013.04.019.

da Rosa, G., Alba, D.F., Silva, A.D., Gris, A., Mendes, R.E., Mostardeiro, V.B., Lopes, T.F., Schetinger, M.R.C., Stefani, L.M., Lopes, M.T., Boiago, M.M., da Silva, A.S., 2020. Impact of Escherichia coli infection in broiler breeder chicks: the effect of oxidative stress on weight gain. Microb. Pathog. 139, 103861. https://doi.org/10.1016/j.micpath.2019.103861.

Di Tommaso, P., Chatzou, M., Floden, E.W., Barja, P.P., Palumbo, E., Notredame, C., 2017. Nextflow enables reproducible computational workflows. Nat. Biotechnol. 35, 316–319.

Dobin, A., Davis, C.A., Schlesinger, F., Drenkow, J., Zaleski, C., Jha, S., Batut, P., Chaisson, M., Gingeras, T.R., 2013. STAR: ultrafast universal RNA-seq aligner. Bioinformatics 29, 15–21.

Ewels, P.A., Peltzer, A.., Fillinger, S., Patel, H., Alneberg, J., Wilm, A., Garcia, M.U., Di Tommaso, P., Nahnsen, S., 2020. The nf-core framework for community-curated bioinformatics pipelines. Nat. Biotechnol. 38, 276–278.

Fu, J., Zong, X., Jin, M., Min, J., Wang, F., Wang, Y., 2023. Mechanisms and regulation of defensins in host defense. Signal Transduct. Target Ther. 8, 300. https://doi.org/10.1038/s41392-023-01553-x.

Garcia, P., Wang, Y., Viallet, J., Jilkova, Z.M., 2021. The chicken embryo model: a novel and relevant model for immune-based studies. Front. Immunol. 12:, 79108. https://doi.org/10.3389/fimmu.2021.791081.

Givisiez, P.E.N., Moreira Filho, A.L.B., Santos, M.R.B., Oliveira, H.B., Ferket, P.R., Oliveira, C.J.B., Malheiros, R.D., 2020. Chicken embryo development: metabolic and morphological basis for in ovo feeding technology. Poult. Sci. 99, 6774–6782. https://doi.org/10.1016/j.psj.2020.09.074.

Gorgoulis, V., Adams, P.D., Alimonti, A., Bennett, D.C., Bischof, O., Bishop, C., Campisi, J., Collado, M., Evangelou, K., Ferbeyre, G., Gil, J., Hara, E., Krizhanovsky, V., Jurk, D., Maier, A.B., Narita, M., Niedernhofer, L., Passos, J.F., Robbins, P.D., Schmitt, C.A., Sedivy, J., Vougas, K., von Zglinicki, T., Zhou, D., Serrano, M., Demaria, M., 2019. Cellular senescence: defining a path forward. Cell 179, 813–827. https://doi.org/10.1016/j.cell.2019.10.005.

Hammad, M.O., 2023. Simplified protocol modification of TRIzol method for extraction of high-quality RNA yield from RNase-rich rat pancreas. Process Biochem. 130, 464–471. https://doi.org/10.1016/j.procbio.2023.04.029.

Hao, S., Shi, W., Chen, L., Kong, T., Wang, B., Chen, S., Guo, X., 2024. CATH-2-derived antimicrobial peptide inhibits multidrug-resistant Escherichia coli infection in chickens. Front. Cell Infect. Microbiol. 14, 1390934. https://doi.org/10.3389/fcimb.2024.1390934.

Hashem, M.A., Hassan, A.E.A., Abou-Elnaga, H.M.M., Abdo, W., Dahran, N., Alghamdi, A.H., Elmahallawy, E.K., 2022. Modulatory effect of dietary probiotic and prebiotic supplementation on growth, immuno-biochemical alterations, DNA damage, and pathological changes in E. coli-infected broiler chicks. Front. Vet. Sci. 9, 964738. https://doi.org/10.3389/fvets.2022.964738.

Hu, W., He, Z., Du, L., Zhang, L., Li, J., Ma, Y., Bi, S., 2023. Biomarkers of oxidative stress in broiler chickens attacked by lipopolysaccharide: a systematic review and meta-analysis. Ecotoxicol. Environ. Saf. 266, 115606. https://doi.org/10.1016/j.ecoenv.2023.115606.

Iba, T., Helms, J., Maier, C.L., Ferrer, R., Levy, J.H., 2025. Mitochondrial dysfunction is a major cause of thromboinflammation and inflammatory cell death in critical illnesses. Inflamm. Res. 74, 17. https://doi.org/10.1007/s00011-025-01994-w.

Islam, A., Kagawa, Y., Miyazaki, H., Shil, S.K., Umaru, B.A., Yasumoto, Y., Yamamoto, Y., Owada, Y., 2019. FABP7 protects astrocytes against ROS toxicity via lipid droplet formation. Mol. Neurobiol. 56, 5763–5779. https://doi.org/10.1007/s12035-019-1489-2.

Karamanos, N.K., Theocharis, A..D., Piperigkou, Z., Manou, D., Passi, A., Skandalis, S.S., Vynios, D.H., Orian-Rousseau, V., Ricard-Blum, S., Schmelzer, C.E.H., Duca, L., Durbeej, M., Afratis, N.A., Troeberg, L., Franchi, M., Masola, V., Onisto, M., 2021. A guide to the composition and functions of the extracellular matrix. The FEBS J. 288, 6850–6912. https://doi.org/10.1111/febs.15776.

Khoshneviszadeh, M., Henneicke, S., Pirici, D., Senthilnathan, A., Morton, L., Arndt, P., Kaushik, R., Norman, O., Jukkola, J., Dunay, I.R., 2024. Microvascular damage, neuroinflammation and extracellular matrix remodeling in Col18a1 knockout mice as a model for early cerebral small vessel disease. Matrix Biol. 128, 39–64.

Kim, D., Pertea, G., Trapnell, C., Pimentel, H., Kelley, R., Salzberg, S.L., 2013. TopHat2: accurate alignment of transcriptomes in the presence of insertions, deletions and gene fusions. Genome Biol. 14, R36. https://doi.org/10.1186/gb-2013-14-4-r36.

Kleyn, F.J., Ciacciariello, M., 2021. Future demands of the poultry industry: will we meet our commitments sustainably in developed and developing economies? Worlds Poult. Sci. J. 77, 267–278. https://doi.org/10.1080/00439339.2021.1904314.

Li, W., Li, W., Zhao, Q., Wu, P., Huang, X., Jin, W., Wang, B., Li, S., Liu, W., Zhang, G., Kang, X., 2024. Combined analysis of the microbiome, metabolome and transcriptome of silkie chickens in response to avian pathogenic E. coli (APEC). Microb. Pathog. 189, 106586. https://doi.org/10.1016/j.micpath.2024.106586.

Liu, H., Song, Z., He, X., Zhang, H., 2024. Free iron accumulation and oxidative stress burden induce ferroptotic atrophy of chicken yolk sac during the late embryogenesis. Anim. Res. One Health. 2, 285–299. https://doi.org/10.1002/aro2.74.

Love, M.I., Huber, W.., Anders, S., 2014. Moderated estimation of fold change and dispersion for RNA-seq data with DESeq2. Genome Biol. 15, 1–21.

Morris, G., Gevezova, M., Sarafian, V., Maes, M., 2022. Redox regulation of the immune response. Cell Mol. Immunol. 19, 1079–1101. https://doi.org/10.1038/s41423-022-00902-0.

Nguyen, T.T.T., Allan, B., Wheler, C., Köster, W., Gerdts, V., Dar, A., 2021. Avian antimicrobial peptides: in vitro and in ovo characterization and protection from early chick mortality caused by yolk sac infection. Sci. Rep. 11, 2132. https://doi.org/10.1038/s41598-021-81734-2.

Olsen, R.H., Frantzen, C.., Christensen, H., Bisgaard, M., 2012. An investigation on first-week mortality in layers. Avian Dis. 56, 51–57. https://doi.org/10.1637/9777-051011-Reg.1.

Palmieri, N., Apostolakos, I., Paudel, S., Hess, M., 2023. The genetic network underlying the evolution of pathogenicity in avian Escherichia coli. Front. Vet. Sci. 10, 1195585. https://doi.org/10.3389/fvets.2023.1195585.

Patro, R., Duggal, G., Love, M.I., Irizarry, R.A., Kingsford, C., 2017. Salmon provides fast and bias-aware quantification of transcript expression. Nat. Methods 14, 417–419.

Paudel, S., Apostolakos, I., Vougat Ngom, R., Tilli, G., de Carvalho Ferreira, H.C., Piccirillo, A., 2024. A systematic review and meta-analysis on the efficacy of vaccination against colibacillosis in broiler production. PLoS One 19, e0301029. https://doi.org/10.1371/journal.pone.0301029.

Rezaee, M.S., Liebhart, D.., Hess, C., Hess, M., Paudel, S., 2021. Bacterial infection in chicken embryos and consequences of yolk sac constitution for embryo survival. Vet. Pathol. 58, 71–79. https://doi.org/10.1177/0300985820960127.

Robbins, J.A., von Keyserlingk, M..A., Fraser, D., Weary, D.M., 2016. Invited review: farm size and animal welfare. J. Anim. Sci. 94, 5439–5455. https://doi.org/10.2527/jas.2016-0805.

Robinson, M.D., McCarthy, D..J., Smyth, G.K., 2010. edgeR: a bioconductor package for differential expression analysis of digital gene expression data. Bioinformatics 26, 139–140. https://doi.org/10.1093/bioinformatics/btp616.

Rossiello, F., Herbig, U., Longhese, M.P., Fumagalli, M., d'Adda di Fagagna, F., 2014. Irreparable telomeric DNA damage and persistent DDR signalling as a shared causative mechanism of cellular senescence and ageing. Curr. Opin. Genet. Dev. 26, 89–95. https://doi.org/10.1016/j.gde.2014.06.009.

Shibata, M., Makihara, N., Iwasawa, A., 2023. The yolk sac's essential role in embryonic development. Rev. Agric. Sci. 11, 243–258. https://doi.org/10.7831/ras.11.0_243.

Speake, B.K., Murray, A..M., Noble, R.C., 1998. Transport and transformations of yolk lipids during development of the avian embryo. Prog. Lipid Res. 37, 1–32. https://doi.org/10.1016/s0163-7827(97)00012-x.

Starck, J.M., 2021. Morphology of the avian yolk sac. J. Morphol. 282, 959–972. https://doi.org/10.1002/jmor.21262.

Sweet, M.J., Ramnath, D.., Singhal, A., Kapetanovic, R., 2025. Inducible antibacterial responses in macrophages. Nat. Rev. Immunol. 25, 92–107. https://doi.org/10.1038/s41577-024-01080-y.

Tang, D., Chen, X., Kang, R., Kroemer, G., 2021. Ferroptosis: molecular mechanisms and health implications. Cell Res. 31, 107–125. https://doi.org/10.1038/s41422-020-00441-1.

Taylor, C.T., Scholz, C.C., 2022. The effect of HIF on metabolism and immunity. Nat. Rev. Nephrol. 18, 573–587. https://doi.org/10.1038/s41581-022-00587-8.

Wang, J., Liu, X., Shao, Y., Li, R., Paudel, S., 2025. Decoding the genome and epigenome of avian Escherichia coli strains by R10.4.1 nanopore sequencing. Front. Vet. Sci. 12, 1541964. https://doi.org/10.3389/fvets.2025.1541964.

Westermann, A.J., Vogel, J., 2021. Cross-species RNA-seq for deciphering host-microbe interactions. Nat. Rev. Genet. 22, 361–378. https://doi.org/10.1038/s41576-021-00326-y.

Wiley, C.D., Velarde, M..C., Lecot, P., Liu, S., Sarnoski, E.A., Freund, A., Shirakawa, K., Lim, H.W., Davis, S.S., Ramanathan, A., Gerencser, A.A., Verdin, E., Campisi, J., 2016. Mitochondrial dysfunction induces senescence with a distinct secretory phenotype. Cell Metab. 23, 303–314. https://doi.org/10.1016/j.cmet.2015.11.011.

Wong, E.A., Uni, Z., 2021. Centennial review: the chicken yolk sac is a multifunctional organ. Poult. Sci. 100, 100821. https://doi.org/10.1016/j.psj.2020.11.004.

Yang, B., Lin, Y., Huang, Y., Shen, Y.Q., Chen, Q., 2024. Thioredoxin (Trx): a redox target and modulator of cellular senescence and aging-related diseases. Redox. Biol. 70, 103032. https://doi.org/10.1016/j.redox.2024.103032.

Yang, W.S., Stockwell, B.R., 2016. Ferroptosis: death by lipid peroxidation. Trends Cell Biol. 26, 165–176. https://doi.org/10.1016/j.tcb.2015.10.014.

Ye, X., Hsu, C.-Y., Jia, L., Zhang, X., Magee, C., Whitham, S., Leigh, S., Evans, J.D., Zhang, L., Robinson, K., 2025. Dynamic immune response to Avian Pathogenic Escherichia coli infection in broiler chickens: insights into pro-inflammatory and anti-inflammatory cytokine regulation: cytokine regulation in APEC infected broilers. Poult. Sci. 104, 105029. https://doi.org/10.1016/j.psj.2025.105029.

Yu, G., 2024. Thirteen years of clusterProfiler. The Innovation 5 (6), 100722. https://doi.org/10.1016/j.xinn.2024.100722.